

Title	Dynamic yielding in lithium fluoride and aluminum
Author(s)	Sano, Yukio; Sano, Tomokazu
Citation	Journal of Applied Physics. 2010, 107(4), p. 043506
Version Type	VoR
URL	https://hdl.handle.net/11094/89435
rights	This article may be downloaded for personal use only. Any other use requires prior permission of the author and AIP Publishing. This article appeared in Yukio Sano and Tomokazu Sano, Journal of Applied Physics 107, 043506 and may be found at https://doi.org/10.1063/1.3275503 .
Note	

Osaka University Knowledge Archive : OUKA

<https://ir.library.osaka-u.ac.jp/>

Osaka University

Dynamic yielding in lithium fluoride and aluminum

Cite as: J. Appl. Phys. **107**, 043506 (2010); <https://doi.org/10.1063/1.3275503>

Submitted: 04 May 2009 • Accepted: 24 November 2009 • Published Online: 18 February 2010

Yukio Sano and Tomokazu Sano



View Online



Export Citation

ARTICLES YOU MAY BE INTERESTED IN

Effect of temperature, strain, and strain rate on the flow stress of aluminum under shock-wave compression

Journal of Applied Physics **112**, 073504 (2012); <https://doi.org/10.1063/1.4755792>

Real time synchrotron x-ray diffraction measurements to determine material strength of shocked single crystals following compression and release

Journal of Applied Physics **106**, 033513 (2009); <https://doi.org/10.1063/1.3187929>

Strength of lithium fluoride under shockless compression to 114 GPa

Journal of Applied Physics **106**, 103507 (2009); <https://doi.org/10.1063/1.3259387>

Trailblazers. New

Meet the Lock-in Amplifiers that measure microwaves.

Zurich Instruments [Find out more](#)

Dynamic yielding in lithium fluoride and aluminum

Yukio Sano^{1,a)} and Tomokazu Sano²

¹38-10, Shibatani-Cho, Takatsuki, Osaka 569-1025, Japan

²Department of Manufacturing Science, Graduate School of Engineering, Osaka University, Suita, Osaka 565-0871, Japan

(Received 4 May 2009; accepted 24 November 2009; published online 18 February 2010)

At a time immediately after shock loading, a kink (a weak discontinuity or a discontinuity in slope) occurs at a position in an unsteady portion in a smooth plane wave front in a lithium fluoride single crystal (material III_b) or in 1060-0 aluminum due to the instability of the wave front. After the occurrence of the kink, a zone is produced and broadened with time between a near steady precursor ahead of the kink and a plastic wave behind it in a weak-discontinuity plane wave by the difference in the propagation velocity between them. Stress relaxes in the zone, which is called a follower, and the precursor decay takes place due to the stress relaxation. During the decay process, the large increase in plastic flow occurs in the vicinity of the leading edge of the follower, causes yielding at the leading edge, and stabilizes the weak-discontinuity wave. The stress-strain (σ - ϵ) history caused by the follower rotates clockwise with time around the yield point. The rotation yields different σ - ϵ histories behind the point and therefore different types of the dynamic σ - ϵ relation. Dynamic yield phenomena are illustrated by showing the schematic diagrams of three different types of the dynamic σ - ϵ relation, which are caused by weak-discontinuity plane waves composed of a precursor C, a follower (i) C, (ii) I or II, or (iii) R' or R_b, and a plastic wave C behind the follower. Here C is the contraction (compression) wave, I and II are the degenerate contraction waves I and II, R' is the subrarefaction wave, and R_b is the rarefaction wave. © 2010 American Institute of Physics. [doi:10.1063/1.3275503]

I. INTRODUCTION

Many studies on dynamic yielding have been performed on single crystals. This includes copper,¹ tantalum,² tungsten,³ aluminum,⁴ sodium chloride,⁵ and lithium fluoride (LiF).⁶ The use of single crystals makes for a more meaningful theoretical analysis of the dislocation density as the slip planes are well defined.⁷ The discontinuities in slope of the stress-time profiles observed in some of these studies^{4,6} suggest the occurrence of the precursor decay and the yielding. Gupta and Fowles⁷ studied them from a microscopic point of view and obtained the results that the stress decay in LiF under dynamic loading was strongly influenced both by Mg⁺⁺ impurities and by heat treatments and that for a given defect concentration, the impurity clustering reduced the rate of attenuation of the elastic precursor.

It is interesting to clarify that the discontinuities in slope of stress-time profiles observed are a sign of yielding. To this end, it is required to obtain any evidence revealing that there exists large plastic flow in a follower behind a precursor in a weak-discontinuity plane wave in a crystal. A high dislocation density estimated at the leading edge of the follower becomes an evidence for the existence of the flow. In addition, it is interesting to make a qualitative analysis of the shock-induced stress-strain relation and to make a schematic representation of it. One can promote better understanding of dynamic yielding through these shock-induced responses of

material of interest. Therefore, there has yet to be a comprehensive study of macroscopically clarifying dynamic yield phenomena.

Recently, Sano⁸⁻¹⁰ has theoretically studied the precursor decay in LiF (III_b).⁶ Sano⁸ inferred that a precursor in a weak-discontinuity plane wave front¹¹ was decayed by an evolving follower overtaking the precursor from behind, which appeared in sequence during the decay process as a contraction (compression) wave C, degenerate contraction waves I and II, a subrarefaction wave R', and a rarefaction wave R_b. In addition, he⁸ found from the stress-time (σ - t) profiles measured by Asay *et al.*⁶ that the amplitude of the stress wave [the stress at the rear (impacted surface) of the σ - x profile] reached a maximum at $T \cong 0.05 \mu\text{s}$ after impact and then the stress wave separated from the impacted surface. Here x is the coordinate in the direction of the wave propagation. Sano⁹ quantitatively analyzed a smooth plane wave front growing in the vicinity of the impact surface of the LiF specimen by assuming that the amplitude and the width of the convex strain wave in the wave front increased with time after impact. The analysis indicated that the amplitude of the steady precursor (the stress at its rear) in the wave front increased from the Hugoniot elastic limit (HEL). He⁹ inferred that at the time $t_s (< T)$ when the amplitude had increased to a maximum, a kink (a weak discontinuity or a discontinuity in slope) occurred immediately behind the steady precursor and that the precursor decay began at t_s . The decay curve that began from the maximum amplitude point was referred to as the Sano's decay curve. He⁹ verified the validity of use of the convex strain wave whose amplitude and width increased with time by showing that the stress-

^{a)}Electronic mail: profeme_ys@yahoo.co.jp.

time profile at the impacted surface predicted in the analysis was close to the measured profile. Sano¹⁰ quantitatively analyzed the precursor decay, revealed that the followers C, I, II, R', and R_b appeared in sequence, and thus verified the existence of the five elementary waves theoretically. Sano¹¹ proved a theorem of equivalence on weak discontinuity, which states that if one of the ε - x , u - x , σ - x , ε - t , u - t , and σ - t profiles has a kink, where ε is the strain and u is the particle velocity, then so are all the others. According to this theorem, the kinks observed in the σ - t profiles of Asay *et al.*⁶ indicate that a weak-discontinuity plane wave passes through LiF (III_b). In addition, the drop of the kink with time and a small change with time in the slopes of the almost linear σ - t profiles up to the kinks suggest that the precursor decay is caused by the follower overtaking the precursor.

A part of the work⁸⁻¹¹ described above includes contents useful for the development of the study on dynamic yielding. Some of the contents are necessary to advance this study, so that they are widely applied to this study.

The first purpose in this study is to demonstrate that yielding occurs at the leading edges of the followers C, I, II, R', and R_b during the decay process in LiF (III_b). To this end, whether or not there is large plastic flow at the leading edge of any follower in the process is examined. The second is to understand dynamic yield phenomena profoundly from a macroscopic point of view. The understanding of the phenomena is enhanced through the qualitative analysis and the schematic representation of the shock-induced stress-strain relation, which is termed as a dynamic stress-strain relation. Based on the difference in the stress-strain history behind the yield point, the dynamic relations are classified into three types, which are caused by weak-discontinuity plane waves composed of a precursor C, a follower (i) C, (ii) I or II, or (iii) R' or R_b, and a plastic wave C behind the follower, and they are displayed schematically. The analogy and the difference with the static stress-strain diagram are described.

II. PRECURSOR DECAY IN LiF

In Sec. II A, it is demonstrated that the form of the strain wave in a smooth plane wave front that grows immediately after shock loading is convex upward. In Sec. II B, the analysis of the wave front that was performed using the strain waves of convex forms by Sano⁹ is summarized¹² and then the main results predicted in the analysis are described. In Sec. II C, the cause of occurrence of a weak-discontinuity plane wave is explained. In Sec. II D, the appearance of a follower into the wave is explained, the stability of the wave is examined with the aid of the result of the analysis, the validity of the inference of the precursor decay by Sano⁸ is indicated, and the appearance of the followers C, I, II, R', and R_b is confirmed.

A. Strain waveform

The shock-induced response of a material in the vicinity of the impact interface is not totally elastic because the projectile contacts imperfectly with the specimen for a certain time immediately after impact due to the roughness on both contact surfaces. The contact area between the surfaces

should increase with time. As a result, the mean strain over the whole impacted surface of the specimen increases with time until the surfaces contact perfectly over the whole contact surface. That is, a strain wave of the amplitude (the strain at the impacted surface) of $\delta(t)$ increasing with time t appears near the impacted surface, and it separates from the surface after the amplitude has reached a maximum value. The width of the strain wave $w(t)$ is expressed by $w=c_0t$ to a good approximation in a range of $0 < t \leq T$, where c_0 is the velocity of the leading edge of the strain wave at $t=0$.¹⁰ In many cases, on the other hand, rate $d\delta/dt$ reduces with time. In this situation, if the phase velocity at constant strain is assumed to be the same at any strain between 0 and a maximum amplitude $\delta(T)$, then the strain waveform is convex upward at any time for $0 < t \leq T$. In case of $d\delta/dt = \text{const.}$, that is, when the δ - t profile at the impacted surface ranging from 0 to T is a straight line, the strain waveform is a straight line at any time. Consequently, the strain waveform at any time is largely curved as the profile deviates from a tangent at the initial point at $t=0$ on the profile. As is clear from the explanation above, if the profile is convex upward, it is valid to use convex strain waveforms in the analysis of a smooth plane wave front growing near the impacted surface.

B. Analysis of a smooth plane wave front growing near the impacted surface

For LiF (III_b), the δ - t profile at the impacted surface deviates largely from the tangent at the initial point on the profile,⁹ and the σ - t profiles near the impacted surface measured by Asay *et al.*¹³ indicate that the phase velocity at constant strain does not depend largely on strain. Therefore, as was demonstrated in the preceding section, the strain wave $\varepsilon(x, t)$ (x is the initial position) in the growing smooth plane wave front in the material was expressed by a convex upward function,^{9,12}

$$\varepsilon - \varepsilon_0 = \delta(\tau)(1 - \xi)^{r(\tau)} \quad (0 < \tau \leq 1), \quad (1)$$

where $r > 0$, $\tau = t/T$, and $\xi = x/\zeta$, where $\zeta(t)$ is the location of the leading edge of the wave front expressed by $\zeta \cong c_0t$ and where $\xi=0$ ($x=0$) represents the impacted surface. The subscript 0 refers to the state at the edge. The amplitude was expressed by $\delta(\tau) = d_1(\tau)(\varepsilon_1 - \varepsilon_0)$, where $\delta(0)=0$ or $d_1(0)=0$, and $\delta(1)=\varepsilon_1 - \varepsilon_0$ or $d_1(1)=1$. A functional form $d_1(\tau) = a(k - \tau)^s + b$ was given to $d_1(\tau)$, where $k > 1$, $s > 0$, and $a = [(k-1)^s - k^s]^{-1}$ and $b = k^s[k^s - (k-1)^s]^{-1}$, which were derived from two conditions $d_1(0)=0$ and $d_1(1)=1$. The equation for the particle velocity wave $u(x, t)$ corresponding to the strain wave was derived from the conservation law of mass,

$$[u] = \frac{1}{\omega + 1} (C_1 X^{r+1} + d_1 X^r + C_3 X^{r+1} \log X), \quad (2)$$

where $X = 1 - \xi$, $[u] = (u - u_0)/(u_1 - u_0)_{\xi=0}$, where $(u_1 - u_0)_{\xi=0} = (\omega + 1)c_0(\varepsilon_1 - \varepsilon_0)$, $\omega = C_1(1)$, and C_1 and C_3 are

$$C_1 = [\{d_2 - r_1 d_1/(r+1)\}\tau - r d_1]/(r+1),$$

$$C_3 = [r_1 d_1 / (r + 1)] \tau,$$

where $r_1 = dr/d\tau$ and $d_2 = d(d_1)/d\tau$. The relation $\omega = C_1(1)$ is transformed as

$$\omega + 1 = [d_2(1) + 1 - r_1(1)/\{r(1) + 1\}]/\{r(1) + 1\}.$$

The equation for the stress wave $\sigma(x, t)$ corresponding to the strain wave was derived from the conservation law of momentum [see Eq. (5)].

By extending the piezoelectric current analysis of Graham *et al.*¹⁴ to become applicable also to unsteady plane wave fronts, relation $[u] = [i]$ was derived, where i is the displacement current and $[i] = i/i_1$, where i_1 is the peak value of the current at the impact surface. The values of k and s , and variable $r(\tau)$ were estimated such that the profile at the impact surface of the LiF sample $[u]_{\xi=0}$, calculated from $[u]_{\xi=0} = [C_1(\tau) + d_1(\tau)]/[\omega(\tau) + 1]$, closely fitted the profile $[i]_{x=0}$ and furthermore the calculated time variations $[u]$ near the impact surface were initially parallel to the $[u]_{\xi=0}$. They are $k=10$, $s=20$, and $r=-0.1\tau+0.8$, from which we have $\omega + 1 \approx 0.8$.

The equations for the strain $[\varepsilon]_R$, particle velocity $[u]_R$, and stress $[\sigma]_R$ waves in the growing smooth plane wave front, where $[\varepsilon]_R = \varepsilon/(\varepsilon_1 - \varepsilon_0)$, $[u]_R = u/(u_1 - u_0)_R$, and $[\sigma]_R = \sigma/(\sigma_1 - \sigma_0)_R$, where $(u_1 - u_0)_R = c_0(\varepsilon_1 - \varepsilon_0)$ and $(\sigma_1 - \sigma_0)_R = \rho_0 c_0^2(\varepsilon_1 - \varepsilon_0)$ (ρ_0 is the uniform constant material density at $t=0$), are, respectively, expressed by

$$[\varepsilon]_R = d_1(\tau)(1 - \xi)^{r(\tau)}, \quad (3)$$

$$[u]_R = C_1 X^{r+1} + d_1 X^r + C_3 X^{r+1} \log X, \quad (4)$$

$$[\sigma]_R = D_1 X^{r+2} + D_2 X^{r+1} + D_3 X^r + (D_4 X^{r+2} + D_5 X^{r+1}) \log X + D_6 X^{r+2} (\log X)^2. \quad (5)$$

As for the expressions for coefficients D_1 through D_6 , see Ref. 9.

Figure 1 shows seven sets of the $[\varepsilon]_R$, the $[u]_R$, and the $[\sigma]_R$ waves up to $\tau=1$ calculated from Eqs. (3)–(5).¹² In Fig. 1, $\tau\xi$ is the dimensionless position expressed by $\tau\xi = x/c_0 T$, where $c_0 = 7000$ m/s and $T = 45$ ns. The latter ($T = 45$ ns) was estimated from the data for thin LiF specimens 0.27 and 0.48 mm thick measured by Asay *et al.*⁶ The portion in which the profiles of the three waves coincide is termed as a steady precursor, while the portion in which they do not coincide is termed as an unsteady portion. The heavy solid line is a curve connecting the interfaces between the steady precursors and the unsteady portions. At any time τ in a range of $0 < \tau \leq \tau^*$, the wave front is an elastic wave. Here τ^* is the dimensionless time when the stress amplitude of an elastic wave induced upon impact has reached the HEL $\sigma_H = [(1 - \nu)/(1 - 2\nu)]\sigma_Y$, where σ_Y is the static yield stress and ν is the Poisson ratio. The value of $[\sigma_H]_R$ is about 0.03, which is calculated from $[\sigma_H]_R = \sigma_H/(\sigma_1 - \sigma_0)_R$ using the values of σ_H (calculated using the values of $\nu = 0.3$ and $\sigma_Y = 0.46$ kbar) and $(\sigma_1 - \sigma_0)_R = 26.0$ kbar. At any time after $\tau = \tau^*$, the wave front consists of a steady precursor and an unsteady portion behind: The amplitude of the precursor increases gradually from $\tau = \tau^*$ to $\tau \approx 0.25$ and more rapidly from $\tau \approx 0.25$ to $\tau \approx 0.35$ ($t \approx 16$ ns), while it decreases after $\tau \approx 0.35$. Thus, the

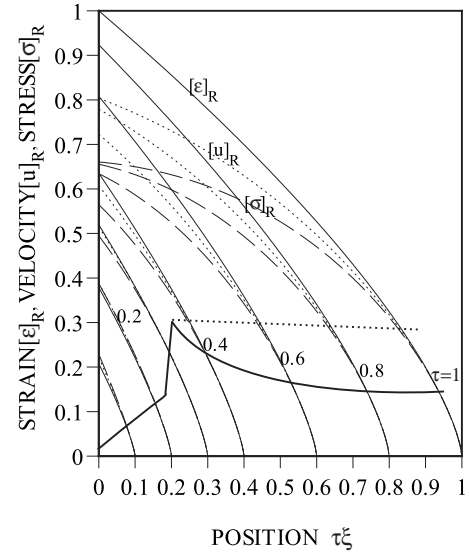


FIG. 1. Strain $[\varepsilon]_R$, particle velocity $[u]_R$, and stress $[\sigma]_R$ waves in a smooth plane wave front calculated for $k=10$, $s=20$, and $r=-0.1\tau+0.8$. The heavy solid line is the curve connecting the rears of the steady precursors. The heavy dotted line is the Sano's decay curve up to $\tau=1$.

amplitude has reached a maximum value at $\tau \approx 0.35$. At the maximum amplitude point, we have $(\tau, [u]_R) = (0.35, 0.31)$ or $(\tau, [u]) = (0.35, 0.39)$ and $x \approx 0.07$ mm, which is calculated from $x = \tau\xi c_0 T$ using three values of $\tau\xi \approx 0.21$ found from Fig. 1, $c_0 = 7000$ m/s, and $T = 45$ ns. Here the value of $[u] = 0.39$ is obtained from $[u] = [u]_R/(\omega + 1)$ using $[u]_R = 0.31$ and $\omega + 1 \approx 0.8$.

C. Occurrence of a kink

As was shown in Fig. 1, the degree of inconsistency of the $[\varepsilon]_R$ - x , $[u]_R$ - x , and $[\sigma]_R$ - x profiles is large as position x is apart from the interface between the steady precursor and the unsteady portion, indicating that the plastic strain component in the unsteady portion, $\varepsilon^p(x, t)$, increases as x is apart from the interface. The increase in the plastic component is also indicated by the property of the unsteady portion (the properties of waves C, I, II, R', and R_b) $\partial \varepsilon^p / \partial t > 0$, which is described in Sec. IIIC. Since the component increases as x is apart from the interface, the stress state is more isotropic in the unsteady portion behind the interface than in the steady portion ahead of it. As a result, the compressibility of material in the unsteady portion changes, and the smooth plane wave front becomes unstable.¹ Due to the instability, a kink occurs at a position in the unsteady portion, and the wave front is separated into a precursor ahead of the kink and an unsteady portion behind it. Figure 1 shows that the precursor is a near-steady wave that is composed of a steady portion up to the heavy solid line and an unsteady portion from the heavy solid line to the heavy dotted line.

D. Precursor decay

After the occurrence of the kink, a zone, which is broadened with time, is produced between the kink and the leading edge of the plastic wave in the unsteady portion by the propagation velocity of the precursor that is faster than that of the plastic wave. Stress relaxation occurs in the zone (the

follower), and the precursor is decayed by the progress of the kink into it during the relaxation process, which means that the follower overtakes the precursor in the decay process.

Sano⁹ obtained a precursor decay curve for stress assuming that a kink occurs at the maximum amplitude point of the steady precursor in the smooth wave front at $\tau \approx 0.35$ and inferring that a weak-discontinuity wave propagates after $\tau \approx 0.35$. In Fig. 1, the Sano's decay curve for stress that starts from the maximum point at $\tau \approx 0.35$ is shown by a heavy dotted d line. The decay curve passes through the unsteady portions behind the steady precursors in the plane wave fronts that were calculated assuming to be smooth also after $\tau \approx 0.35$, indicating that the weak-discontinuity wave having a kink at an intersection point of the heavy dotted curve and the stress wave is stable, which means that the inference of Sano⁹ described above is valid. The stability of the weak-discontinuity wave is verified by the kinks observed in the σ - t profiles of Asay *et al.*⁶ Sano⁸ inferred that the precursor decay was caused by the follower overtaking the precursor. The validity of the decay is indicated by the progress of the kink into the precursor described above and is verified by the drop of the kink in the profile of Asay *et al.*⁶ with time.

Sano¹⁰ quantitatively analyzed the precursor decay and indicated that the follower C appeared from $t = 0.015$ to $0.055 \mu\text{s}$, the follower I from 0.055 to $0.057 \mu\text{s}$, the follower II from 0.057 to $0.063 \mu\text{s}$, the follower R' from 0.063 to $0.095 \mu\text{s}$, and the follower R_b after $0.095 \mu\text{s}$. Sano and Sano¹⁵⁻¹⁷ obtained the same result as that of Sano¹⁰ using the inequalities for the dislocation density at the leading edge of the follower derived by Sano.⁸

III. DYNAMIC YIELDING IN LIF

In Sec. III A, it is indicated that there is a large plastic flow near the leading edge of the follower. In Sec. III B, to enhance the understanding of dynamic yielding, the dynamic stress-strain relation is qualitatively analyzed using the properties of the followers and three different types of the relation analyzed are schematically shown.

A. Plastic flow

Sano and Sano^{15,16} calculated the dislocation density N_{mi} at the leading edge of the follower on the Sano's decay curve (see Appendix). The results of calculation indicated that the density decreased rapidly from a maximum value $N_{mi} \approx 2.0 \times 10^{11} \text{ m}^{-2}$ at the beginning of the decay process ($t_s = 0.015 \mu\text{s}$) to a value $N_{mi} \approx 0.65 \times 10^{11} \text{ m}^{-2}$ at $t = 0.3 \mu\text{s}$ and then slowly to a value $N_{mi} \approx 0.59 \times 10^{11} \text{ m}^{-2}$ at $t = 1.0 \mu\text{s}$.¹⁵⁻¹⁷ The values of the densities of $(2.0-0.59) \times 10^{11} \text{ m}^{-2}$ obtained are considerably larger than those of $(2.1-1.3) \times 10^{10} \text{ m}^{-2}$ estimated at the rear of the precursor,^{15,16} suggesting that in the vicinity of the leading edge of the follower, there is a plastic flow ($\partial \varepsilon^p / \partial t$) that is large enough to cause yielding at the edge. The sudden change in the stress state near the leading edge caused by the flow would stabilize the weak-discontinuity plane wave.

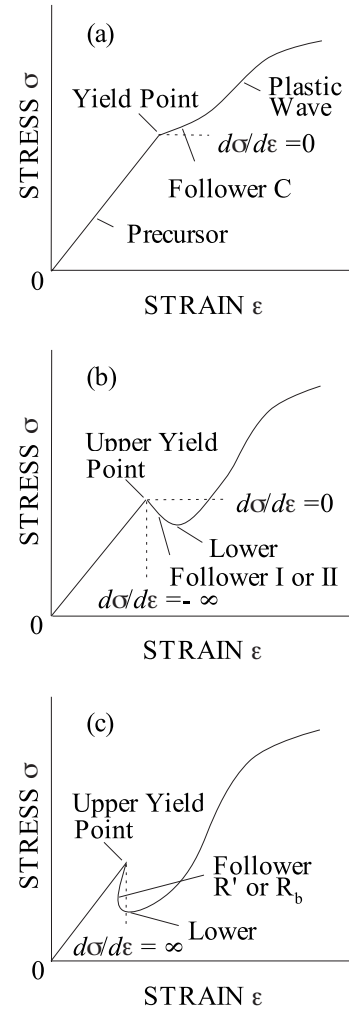


FIG. 2. Schematic diagrams of (a) first, (b) second, and (c) third types of the dynamic stress (σ)-strain (ε) relation in LiF III_b. The first type is caused by a weak-discontinuity plane wave composed of a precursor, a follower C, and a plastic wave, the second by that composed of a precursor, a follower I or II, and a plastic wave, and the third by that composed of a precursor, a follower R' or R_b, and a plastic wave. The slopes of the tangent at the point on the σ - ε relation immediately behind the kink for the followers C, I, II, R', and R_b, $(d\sigma/d\varepsilon)_C$, $(d\sigma/d\varepsilon)_I$, $(d\sigma/d\varepsilon)_{II}$, $(d\sigma/d\varepsilon)_{R'}$, and $(d\sigma/d\varepsilon)_{R_b}$, satisfy inequalities $(d\sigma/d\varepsilon)_C > 0$, $0 > (d\sigma/d\varepsilon)_I > (d\sigma/d\varepsilon)_{II}$, $(d\sigma/d\varepsilon)_{I-II} > (d\sigma/d\varepsilon)_{II} > -\infty$, $\infty > (d\sigma/d\varepsilon)_{R'} > (d\sigma/d\varepsilon)_{R'-R_b}$, and $(d\sigma/d\varepsilon)_{R_b} < (d\sigma/d\varepsilon)_{R'-R_b}$, respectively. Here $(d\sigma/d\varepsilon)_{I-II}$, is the slope at the time immediately before the follower I changes into the follower II.

B. Qualitative analysis of the dynamic stress-strain relation

The upper yield point on the dynamic stress-strain (σ - ε) curve is defined as a local maximum point from which the stress begins to drop due to the plastic strain component ε^p that increases largely. The precursor, which is the wave C, has the property of $\partial \varepsilon / \partial t > 0$, $\partial \varepsilon^p / \partial t > 0$, and $\partial \sigma / \partial t > 0$.¹⁰ It is found from the property of the wave C that if the follower is also the wave C, both the stress-strain history caused by the precursor and that by the follower have positive gradients ($d\sigma/d\varepsilon > 0$). A first type of the σ - ε relation, which is caused by a weak-discontinuity plane wave composed of a precursor, a follower C, and a plastic wave, is schematically shown in Fig. 2(a). The curve, as shown, has a kink at the point where two σ - ε histories by the precursor and the follower

connect. The connection point of both histories is a yield point, but the point is not an upper yield point because it is not a local maximum. In fact, as is found from the ε - t and σ - t profiles calculated by Sano¹⁰ under the inference that the angle of incidence of the strain wave in the follower C increases continuously with time, the slope of the tangent at the point on the σ - ε relation immediately behind the kink, $(d\sigma/d\varepsilon)_C$, decreases continuously with time from a positive value at the beginning of the decay process to a value of 0.

The followers I and II have the same property of $\partial\varepsilon/\partial t > 0$, $\partial\varepsilon^p/\partial t > 0$, and $\partial\sigma/\partial t < 0$. The σ - ε histories caused by the two kinds of the followers have negative gradients ($d\sigma/d\varepsilon < 0$). Therefore, a sequence of the histories caused by the precursor and the follower I or II has a kink at their connection point. The point is a local maximum. According to the definition, it is an upper yield point. A second type of the relation, which is caused by a weak-discontinuity plane wave composed of a precursor, a follower I or II, and a plastic wave, is schematically shown in Fig. 2(b). The diagram of this type is schematically analogous to the static σ - ε diagram up to the tensile strength for mild steel. As is found from the ε - t and σ - t profiles for the follower I calculated by Sano,¹⁰ the slope of the tangent at the point immediately behind the kink, $(d\sigma/d\varepsilon)_I$, decreases continuously with time from a value of 0 to the value of $(d\sigma/d\varepsilon)_{I-II}$, where $(d\sigma/d\varepsilon)_{I-II}$ is the slope at the time immediately before the follower I changes into the follower II. On the other hand, the slope $(d\sigma/d\varepsilon)_{II}$ for the follower II does from the value of $(d\sigma/d\varepsilon)_{I-II}$ to a value of $-\infty$.¹⁰

The followers R' and R_b have the same property of $\partial\varepsilon/\partial t < 0$, $\partial\varepsilon^p/\partial t > 0$, and $\partial\sigma/\partial t < 0$. The σ - ε histories caused by the two kinds of the followers have positive gradients larger than that by the precursor. Therefore, as seen in the curve shown in Fig. 2(c), it has a kink at the connection point of the histories by the precursor and the follower R' or R_b. Figure 2(c) schematically shows a third type, which is represented by a sequence of three histories caused by a precursor, a follower R' or R_b, and a plastic wave. The diagram of this type is not schematically analogous to any static σ - ε diagram, so that it is characteristic of the dynamic relation. Even though the slope of the history caused by the follower is positive, the connection point is a local maximum, so that it is an upper yield point. For the follower R', the slope of the tangent at the point immediately behind the kink, $(d\sigma/d\varepsilon)_{R'}$, decreases continuously with time from a value of ∞ .¹⁰ The same is true of the follower R_b except that the decrease in the slope $(d\sigma/d\varepsilon)_{R_b}$ starts from a value of $(d\sigma/d\varepsilon)_{R'-R_b}$.

The lower yield point on the dynamic σ - ε curve is defined as a local minimum point at which the stress turns to a rise. The point where the σ - ε history caused by the follower I, II, R', or R_b connects with that by the plastic wave behind the follower is a local minimum. According to the definition, the connection point of both histories is a lower yield point.

IV. DYNAMIC YIELDING IN ALUMINUM

The stress-time profiles measured by Arvidsson *et al.*⁴ in 1060-0 aluminum specimens of thickness b ranging from

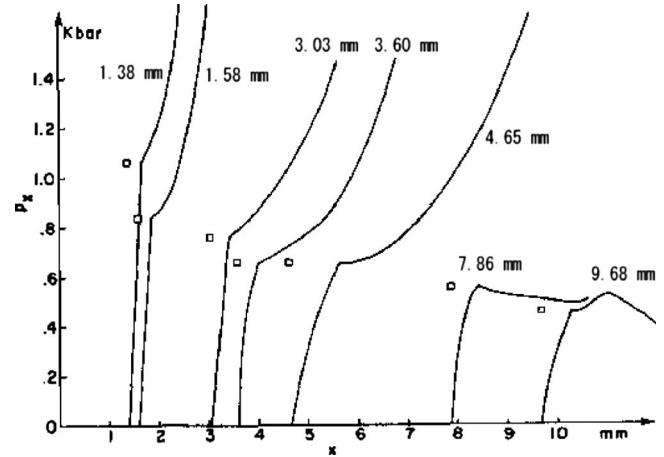


FIG. 3. Stress-time profiles measured by Arvidsson *et al.* (Ref. 4) for 1060-0 aluminum specimens of thicknesses 1.38, 1.58, 3.03, 3.60, 4.65, 7.86, and 9.68 mm.

1.38 to 9.68 mm are shown in Fig. 3. Any profile shown has a clear kink. As described in Sec. I, the theorem of equivalence on weak discontinuity¹¹ reveals that a weak-discontinuity plane wave, which is composed of a precursor, a follower, and a plastic wave, propagates through this material. As is the case with LiF (III_b), the kink drops with time, suggesting that the precursor decay in 1060-0 aluminum is similar to that in LiF (III_b).

The quantitative analysis of the precursor decay, which is similar to that performed by Sano^{10,17} to specify the kind of the follower that appears during the decay process in LiF (III_b), is not made here. Instead, the kind of the follower is found out in an easy method using the following inequalities found by Sano⁸ that hold at a fixed position h for the wave C, for the wave I, and for the waves II, R', and R_b, respectively,

$$F_S > F_Y, \quad F_Y < 0,$$

$$F_S > F_Y > 0,$$

$$F_Y > F_S, \quad F_Y > 0,$$

where $(-F_Y)$ is the slope of the tangent at the point on the $\sigma(t)$ profile immediately after the kink, $d\sigma/dt$, and $-F_S = d\sigma_i/dt$, where $\sigma_i(t)$ is the decay curve for stress (see Appendix). The profiles for the specimens of thickness ranging from 1.38 to 4.65 mm show $F_Y < 0$, so that the follower passing through any position h between 1.38 and 4.65 mm is inferred to be the wave C.⁸ The profile for the specimen of $b = 7.86$ mm shows $F_Y > F_S$ and $F_Y > 0$, so that the follower passing through the position $h = 7.86$ mm is inferred to be the wave II, R', or R_b. As is found from the observation of the whole profiles ranging from 1.38 to 9.68 mm, $(-F_Y)$ becomes continuously small with time. Although no profile is shown in an interval from 4.65 to 7.86 mm, it is inferred from the time variation in the slope described immediately above and the similar variation in LiF (III_b) that the slope also decreases continuously in this interval. Since we have $F_Y < 0$ for the profile at $h = 4.65$ mm and $F_Y > F_S$ and $F_Y > 0$ for the profile at $h = 7.86$ mm, which was mentioned above, there should be the profiles that satisfy inequalities

$0 < F_Y < F_S$ in a part of the interval. That is, the follower passing through any position in the part should be the wave I. Therefore, it is inferred from the profiles in Fig. 3 that the followers C, I, and II, the followers C, I, II, and R', or the followers C, I, II, R', and R_b appeared in the decay process. The follower R_b should appear in the specimens thicker than 9.68 mm.

As described above, the precursor decay in 1060-0 aluminum is similar to that in LiF (III_b). This similarity indicates that the dynamic σ - ε relations for both materials are schematically similar. Therefore, both the dynamic σ - ε relation and the dynamic yield phenomena in 1060-0 aluminum are illustrated by the schematic diagrams of three types shown in Fig. 2.

V. CONCLUSIONS

For LiF (III_b), it was demonstrated that yielding occurred at the leading edges of the followers C, I, II, R', and R_b which in sequence overtook the near-steady precursor during the decay process. The stress-strain (σ - ε) history caused by the follower rotates clockwise with time around the yield point. The rotation yielded different types of the dynamic σ - ε relation. The relations were classified into three types. The first type is caused by a weak-discontinuity plane wave composed of a precursor, a follower C, and a plastic wave, the second by that composed of a precursor, a follower I or II, and a plastic wave, and the third by that composed of a precursor, a follower R' or R_b, and a plastic wave. There is a yield point on the first type curve, while there is an upper and a lower yield point on the second and the third type curve, respectively. The second type diagram is schematically analogous to the static σ - ε diagram up to the tensile strength for mild steel. The third is characteristic of the dynamic σ - ε relation. The same is true of the dynamic σ - ε relation and the dynamic yield phenomena in 1060-0 aluminum. This study enhances not only the understanding of dynamic yield phenomena in solids but also thinking faculty required in formulating time-dependent constitutive relations that describe dynamic behaviors of solids.

APPENDIX: DISLOCATION DENSITY

Using the equations for the strain, particle velocity, and stress waves in the follower,¹⁰ Sano and Sano¹⁵⁻¹⁷ derived an equation for the relaxation function $F_i[(\partial e^p / \partial q)_{x,x=x_i}]$ at the

leading edge of the follower on the decay curve, where e^p is the plastic component of natural strain e and $q = t - t_s$ (t_s is the time when a kink has occurred),

$$F_i = -(\rho_0 c \dot{v}_i + \dot{\sigma}_i),$$

where the dots on the variables refer to differentiation with respect to q , $v_i = c\varepsilon_i + (\dot{\varepsilon}_i \xi_f + \varepsilon_i \dot{\xi}_f)/2$, and $\sigma_i = \rho_0(c^2 \varepsilon_i - A \xi_f - B \xi_f^2 - D \xi_f^3)$,¹⁰ where $v_i(q)$ and $\sigma_i(q)$ are the decay curves for particle velocity and stress, respectively, and ξ_f is the thickness of the precursor. As for the expressions for the c - q , ε_i - q , and ξ_f - q relations and the coefficients $A(q)$, $B(q)$, and $D(q)$, see Ref. 10. The equation for the dislocation density N_{mi} at the leading edge is expressed by

$$N_{mi} = \eta_i F_i,$$

where $\eta_i = 10/(63v_{di})$ GPa⁻¹ m⁻² s for LiF (III_b), where v_{di} is the average dislocation velocity given by $v_{di} = v_s \exp(-D/\tau_{ri})$, where τ_{ri} is the resolved shear stress given by $\tau_{ri} = (221/760)\sigma_i$, D is the drag stress, and v_s is the shear wave velocity, whose value is 3280 m/s.⁶ The value of D is 0.036 GPa.¹⁵⁻¹⁷

¹O. E. Jones and J. D. Mote, *J. Appl. Phys.* **40**, 4920 (1969).

²P. P. Gillis, K. G. Hoge, and R. J. Wasley, *J. Appl. Phys.* **42**, 2145 (1971).

³T. E. Michaels, Ph.D. thesis, Washington State University, 1972.

⁴T. E. Arvidsson, Y. M. Gupta, and G. E. Duvall, *J. Appl. Phys.* **46**, 4474 (1975).

⁵W. J. Murri and G. D. Anderson, *J. Appl. Phys.* **41**, 3521 (1970).

⁶J. R. Asay, G. R. Fowles, G. E. Duvall, M. H. Miles, and R. F. Tinder, *J. Appl. Phys.* **43**, 2132 (1972).

⁷Y. M. Gupta and G. R. Fowles, in *Metallurgical Effects at High Strain Rates*, edited by R. W. Rohde, B. M. Butcher, J. R. Holland, and C. H. Karnes (Plenum, New York, 1973), p. 367.

⁸Y. Sano, *J. Appl. Phys.* **77**, 3746 (1995).

⁹Y. Sano, *J. Appl. Phys.* **85**, 7616 (1999).

¹⁰Y. Sano, *J. Appl. Phys.* **88**, 1818 (2000).

¹¹Y. Sano and I. Miyamoto, *J. Math. Phys.* **41**, 6233 (2000).

¹²Y. Sano and T. Sano, in *Shock Compression of Condensed Matter-2007*, edited by M. L. Elert, M. D. Furnish, R. Chau, N. C. Holmes, and J. Hguyen (AIP, New York, 2007), p. 263.

¹³J. R. Asay, Ph.D. thesis, Washington State University, 1971.

¹⁴R. A. Graham, F. W. Neilson, and W. B. Benedick, *J. Appl. Phys.* **36**, 1775 (1965).

¹⁵Y. Sano and T. Sano, in *Shock Compression of Condensed Matter-2007*, edited by M. L. Elert, M. D. Furnish, R. Chau, N. C. Holmes, and J. Hguyen (AIP, New York, 2007), p. 275.

¹⁶Y. Sano and T. Sano, *J. Appl. Phys.* **106**, 023534 (2009).

¹⁷Y. Sano and T. Sano, in *Shock Compression of Condensed Matter-2007*, edited by M. L. Elert, M. D. Furnish, R. Chau, N. C. Holmes, and J. Hguyen (AIP, New York, 2007), p. 279.